IEEE Access
Multidisciplinary ⋮ Rapid Review ⋮ Open Access Journal

Received 24 April 2023, accepted 25 May 2023, date of publication 5 June 2023, date of current version 14 June 2023.

Digital Object Identifier 10.1109/ACCESS.2023.3282706

RESEARCH ARTICLE

Dual-Band End-Fire Four-Element MIMO Antenna Array Using Split-Ring Structure for mm-Wave 5G Applications

MOHAMED ABOUALALAA[1], (Member, IEEE), AND ISLAM MANSOUR[2]
[1]Microstrip Department, Electronics Research Institute (ERI), Cairo 11843, Egypt
[2]Electrical Engineering Department, Shoubra Faculty of Engineering, Benha University, Cairo 11629, Egypt

Corresponding author: Mohamed Aboualalaa (m.aboualalaa@eri.sci.eg)

ABSTRACT This paper presents a dual-band split-ring structure that provides end-fire radiation characteristics for multi-input multi-output (MIMO) mm-wave 5G applications. The proposed single antenna element consists of a main split-ring resonator (SRR) directly fed using a high impedance microstrip transmission line. A lamda/4 transformer is employed to match the high impedance transmission line with a 50-ohm line. Two symmetric parasitic SRRs are used as directing elements to give end-fire radiation properties for the introduced antenna at the first resonant frequency. The parasitic SRRs are also utilized to produce the second resonant frequency by establishing a capacitive link with the main SRR. The single element antenna radiates at 24.5 and 28.5 GHz. A cross-shaped MIMO structure composed of four elements of the proposed antenna is introduced to improve the isolation of the MIMO system due to its orthogonal polarization characteristics. The proposed MIMO demonstrates acceptable values of gain and radiation efficiency, reaching 9.8 dB and 93%, respectively, at the first resonant frequency, and 8.7 dB and 95%, respectively, at the second band. MIMO performance is also studied, and the proposed MIMO system provides a very low envelope correlation coefficient of lower than 10^{-4} over the two operating frequency bands. A diversity gain is also calculated, it is around 10 dB over the two operating bands. The proposed high-isolation dual-band cross-shaped MIMO array is a promising candidate for millimeter-wave 5G applications.

INDEX TERMS Diversity gain (DG), envelope correlation coefficient (ECC), fifth generation (5G), millimeter-wave (MMW), multiple-input-multiple-output (MIMO), polarization diversity, split ring resonator (SRR).

I. INTRODUCTION

In recent years, fifth-generation (5G) wireless communication systems have received increasing attention due to the continuous expansion of wireless communication systems, such as smartphones, tablets, and telemedicine. 5G wireless communication systems help increasing the channel capacity, data rate, improving system efficiency. One of the key technologies driving 5G communication systems is multiple-input multiple-output (MIMO) technology. MIMO wireless technology can highly improve data transmission rates, reception probability, and link reliability of wireless systems by utilizing multi-path data transmission and reception through multiple antenna elements at the transmitting and receiving sides [1], [2], [3], [4], [5], [6], [7], [8], [9].

Recently, various MIMO antenna arrays have been introduced [10], [11], [12], [13], [14], [15]. In [10], a dual-band MIMO array using a multi-slot decoupling technique for sub-6GHz fifth generation mobile communication applications is presented. It uses a multi-slot structure to improve the isolation between the MIMO antenna elements, achieving 15.5dB and 19dB isolations over the two resonant frequency bands. Chang et al. proposed a polarization-orthogonal dual antenna pair for 5G MIMO smartphones at sub-6 GHz band, using metallic bezels [11]. The antenna pair offers an isolation of over 20.1dB. In [12], a dual-polarized eight-port MIMO

The associate editor coordinating the review of this manuscript and approving it for publication was Hassan Tariq Chattha.

antenna array for 5G communication is introduced, consisting of two different four-antenna of L-shaped and C-shaped coupled-fed monopole slot to exhibit orthogonal polarization. The isolation between antennas is better than 12.5 dB. An eight-port/four-resonator slot antenna MIMO array with dual-polarized function for 5G mobile terminals is proposed in [13]. Square-ring slot radiators, fed by pairs of microstrip feed lines, are used to radiate at a frequency of 3.6GHz; a pair of open-ended circular-ring parasitic structures is fixed through each square-ring slot radiator to enhance the isolation between the adjunct microstrip feed lines, achieving an isolation of more than 25 dB. Z. Ren et. al. presented a self-decoupled compact antenna design for 5G MIMO in mobile terminals at a frequency of 3.5 GHz with isolation better than 17 dB [14]. A two-port same-polarized rectangular patch antenna, based on generating two out-of-phase TM_{10} modes, provides an isolation higher than 15 dB, as discussed in [15]. In [16], a metasurface structure is used for enhancing the bandwidth, gain, and isolation of a triple-band MIMO system with minimum isolation of 17, 18, and 32 dB at the three resonant frequencies. Ameen et al. introduced a split-ring resonator loaded self-decoupled dual-band MIMO antenna with a minimum isolation of 15 dB for the two frequency bands [17]. A wideband circularly-polarized high-gain diversity antenna is proposed in [18]. It uses a metasurface reflector to get a maximum antenna gain of 7.02 dBic and isolation better than 14.5 dB.

In addition, many other MIMO antenna arrays are used to improve the isolation between antenna elements [19], [20], [21], [22], [23], [24], [25]. However, this paper proposes a novel design of dual-band end-fire cross-shaped MIMO antenna array, using split-ring resonators for mm-wave 5G applications, with a minimum isolation of 33 dB and a very low envelope correlation coefficient, it reaches 10^{-4} over the two operating frequency bands. Section II demonstrates the antenna structure and its geometrical parameters. The results of the antenna, including the reflection and transmission coefficients, the parametric study of the main antenna parameters, as well as the radiation characteristics of the proposed antenna design, are illustrated in Section III. The MIMO system is tested and discussed in section IV, with results revealed in Section V. Finally, the conclusion is presented in Section VI.

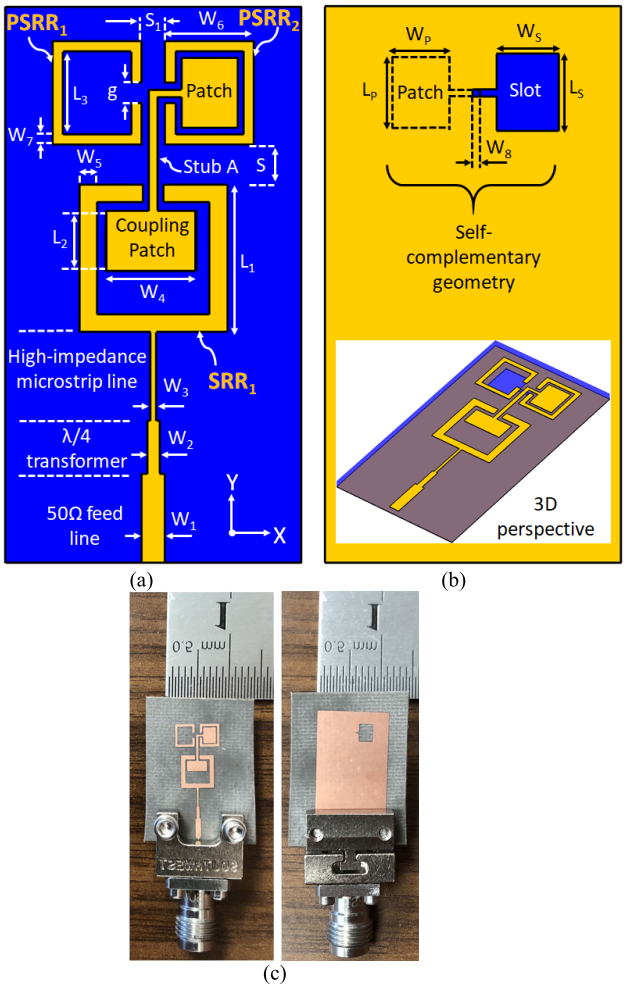

FIGURE 1. Antenna structure (a) front view, (b) back view, and (c) prototype of the fabricated antenna design, $L_1 = 5$ mm, $L_2 = 1.5$ mm, $L_3 = 2.8$ mm, $L_p = 2.38$ mm, $L_S = 2.6$ mm, $W_1 = 0.8$ mm, $W_2 = 0.43$ mm, $W_3 = 0.2$ mm, $W_4 = 3.05$ mm, $W_5 = 0.6$ mm, $W_6 = 3$ mm, $W_7 = 0.35$ mm, $W_8 = 0.3$ mm, $W_P = 1.9$ mm, $W_S = 2.1$ mm S = 2.14 mm, $S_1 = 1.3$ mm, and g = 0.7 mm.

II. PROPOSED ANTENNA DESIGN

The configuration of the proposed dual-band end-fire antenna is illustrated in Fig. 1. The antenna is comprised of three separate split-ring resonators (SRRs). The primary SRR, known as SRR_1, is fed directly through a high-impedance microstrip line as a result of its high input impedance. To achieve impedance matching between the 50 Ω transmission line and the high-impedance microstrip line, a λ/4 transformer is utilized. SRR_1 is designed to radiate at the first resonance frequency (f_1). $PSRR_1$ and $PSRR_2$ are two parasitic split ring resonators that work as directors to direct the main beam in the end-fire direction of the antenna. The two symmetric PSRRs ($PSRR_1$ and $PSRR_2$), which are responsible for the end-fire radiation characteristics, are also utilized to generate the second resonant frequency (f_2) by exciting them using capacitive coupling through the main SRR_1 with the coupling patch and stub A, as demonstrated in Fig. 1(a). Stub A is loaded with a capacitive load to improve the matching at the second resonance frequency. Moreover, the pair of parasitic resonators use a self-complementary structure for adjusting the antenna matching and obtaining a broad bandwidth at the second resonance frequency. As illustrated in Fig. 1(b), the self-complementary structure comprises of a top-layer patch and a bottom-layer slot. In the case of operation at f_2, the main SRR1 is used as a reflector to obtain end-fire radiation at the second frequency band. The antenna design is printed on Rogers RT/Duroid RO5880 material, utilizing a substrate with a thickness (h) of 0.508 mm, a dielectric constant (ε_r) of 2.2, a copper thickness (t) of 35 μm, and a dielectric loss

tangent (tanδ) of 0.0009. The individual unit of the antenna possesses a compact form factor with dimensions of 10 mm × 18 mm × 0.508 mm, resulting in a low profile. The caption of Fig. 1 illustrates the fine-tuned geometric dimensions of the single element of the proposed antenna, while Fig. 1(c) showcases the physical prototype of the fabricated antenna.

III. ANTENNA RESULTS

A. ANTENNA REFLECTION COEFFICIENT

Starting with the single-element antenna, the fundamental properties of the proposed dual-band antenna with various design parameters have been studied, and the simulation, as well as the measurement results, are presented. SRR_1 is designed to radiate at 24.5 GHz band (f_1). While the two parasitic PSRRs ($PSRR_1$ and $PSRR_2$), are designed to provide a wide bandwidth at 28.5 GHz frequency band (f_2). The coupling patch, in addition to stub A, is used to excite PSRRs by a capacitive coupling between SRR_1 and PSRRs. Employing the complementary structure, in addition to adjusting the distance between the two parasitic SRRs, a wide band operation can be obtained. Fig. 2 displays the simulated and measured results of the reflection coefficient for the proposed single-element antenna. The proposed antenna covers dual-band operation, from 23.7 to 25.55 GHz and from 27.8 to 31.8 GHz, with an impedance bandwidth of 7.5%, and 11%, respectively. There is a slight discrepancy between the numerical and the measured results, which could be caused by the fabrication tolerance and fixing the mm wave connector. The measurement of the reflection coefficient was conducted using a vector network analyzer manufactured by Rohde & Schwarz (VNA) ZVA67.

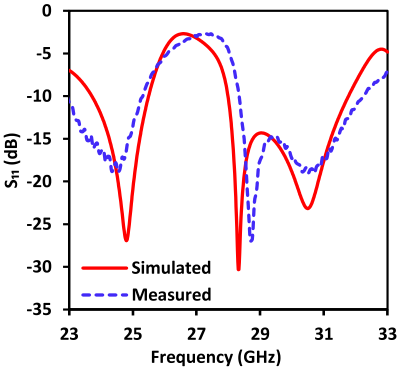

FIGURE 2. Numerical and experimental findings of reflection coefficient for the proposed antenna.

Figs. 3(a)-(c) illustrate the effects of changing different parameters of the proposed antenna configuration, such as the separation distance (S) between SRR_1 and the two symmetric PSRRs shown in Fig. 3(a), as well as the separation distance (S_1) between the two PSRRs and the length of the coupling patch (L_2) located inside SRR_1, as shown in Figs. 3(b) and 3(c), respectively. The matching at the higher frequency band can be optimized using the proper dimensions of (S, S_1, and L_2). To further demonstrate the

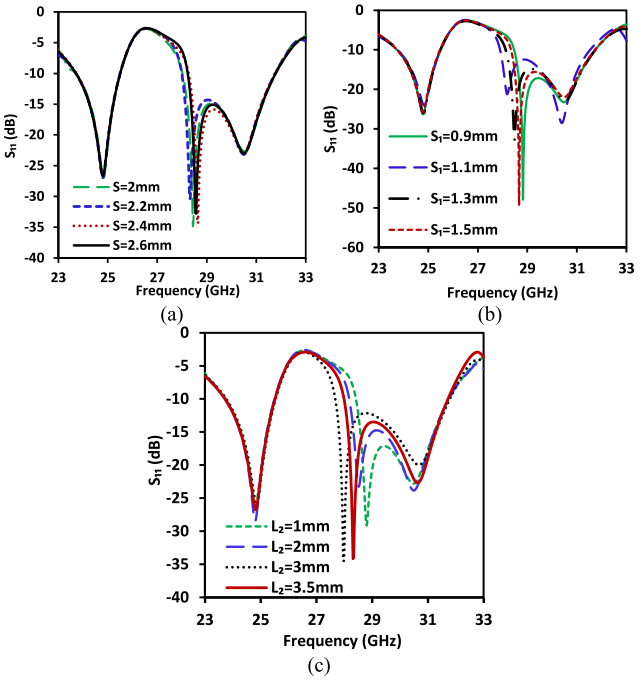

FIGURE 3. Parametric study of antenna main parameters (a) S_{11} at various values of S, (b) S_{11} at various values of S_1, and (c) S_{11} at various values of L_2.

operational concept of the suggested antenna design, the surface current distribution of the proposed antenna at the two resonant frequencies is presented in Fig. 4. It is clear from Fig. 4 that SRR_1 is responsible for the first frequency band, where the current is concentrated on it. On the other hand, the combination of $PSRR_1$ and $PSRR_2$, with the help of the complementary structure, is used to achieve wideband operation at the second operating frequency band.

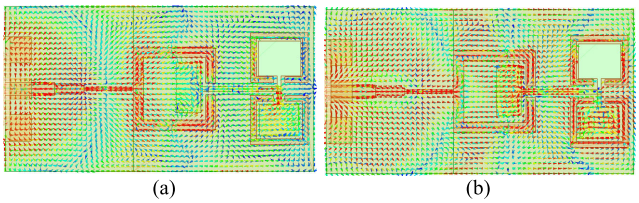

FIGURE 4. Surface current distribution at (a) 24.5 GHz and (b) 28.5 GHz.

B. RADIATION CHARACTERISTICS OF THE PROPOSED ANTENNA

The proposed antenna exhibits end-fire radiation characteristics at the first band where the PSRRs are used as directors. At the second band, the main SRR is utilized as a reflector to achieve end-fire radiation when PSRRs radiate at the second frequency band. At the first resonant frequency, Fig. 5 displays the shapes of the radiation patterns observed in the three orthogonal planes (i.e., XY-plane at $\theta = 90°$, XZ-plane at $\phi = 0°$, and YZ-plane at $\phi = 90°$) through 3D and normalized 2D polar plots. Fig. 6 likewise exhibits the 3D and normalized

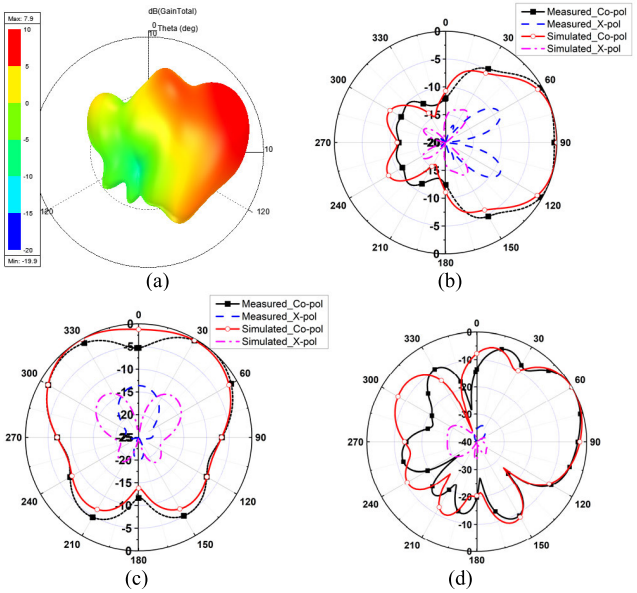

FIGURE 5. 3D and normalized 2D polar plots of the radiation patterns for a single element at f_1 (a) 3D radiation pattern (b) 2D at $\theta = 90°$, (c) 2D at $\phi = 0°$, (d) 2D at $\phi = 90°$.

2D radiation patterns of the suggested antenna at the second resonant frequency. The radiation patterns shown in both Figs. 5 and 6 clearly reveal that the antenna is capable of end-fire radiation properties at the two bands of operation. The gains of the antenna are measured at 7.9 and 7.5 dB with radiation efficiencies of 92% and 95% at 24.5 and 28.5 GHz, respectively. Ansys HFSS as well as measured results of 2D polar plot for radiation patterns are presented.

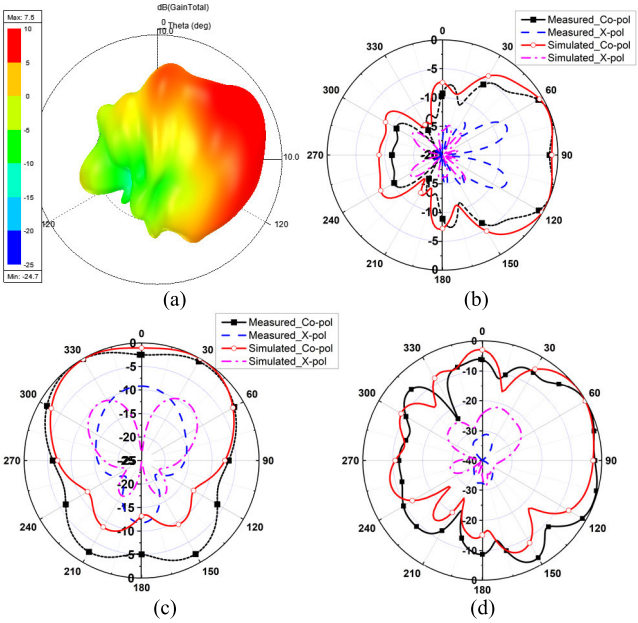

FIGURE 6. 3D and normalized 2D polar plots of the radiation patterns for single element at f_2 (a) 3D radiation pattern (b) 2D at $\theta = 90°$, (c) 2D at $\phi = 0°$, (d) 2D at $\phi = 90°$.

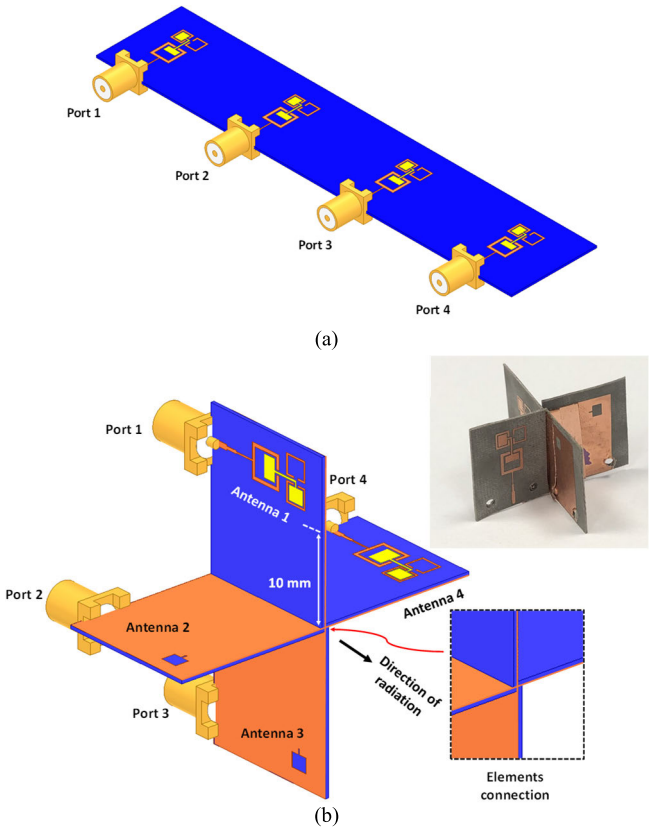

FIGURE 7. Geometry of the MIMO system (a) planar MIMO structure, and (b) proposed cross-shaped MIMO structure.

IV. MIMO SYSTEM

Firstly, we studied a planar MIMO array consisting of four antenna elements placed on the same axis, as shown in Fig. 7(a). The goal was to obtain radiation from each antenna element in the same direction, taking advantage of the end-fire radiation characteristics. However, the results showed that the isolation between the antennas was insufficient for MIMO applications, with values of around −23 dB and −22 dB at 24.5 GHz and 28.5 GHz, respectively. Therefore, to improve the isolation between the antennas MIMO system, a cross-shaped configuration revealed in Fig. 7(b) is used and implemented to provide polarization diversity, which in turn increases the isolation between antenna elements by getting two orthogonal linearly polarized modes. Moreover, the proposed cross-shaped structure reduces the coupling between antennas by employing the ground plane for each element to act as a barrier. For example, as shown in Fig. 7(b), antenna 1 has a maximum coupling with antenna 3 because they have the same polarization. However, after putting antenna 2 and antenna 4 in the path between antenna 1 and antenna 3, the ground plane for two antennas (antenna 2 and antenna 4) acts as a barrier to reduce the mutual coupling between antenna 1 and antenna 3. Whereas antenna 1 and antenna 2 have lower coupling due to their different polarization. Similarly, antenna 3 and antenna 4

have less mutual coupling because of their orthogonal polarization. In addition, this structure preserves the end-fire radiation characteristics, allowing all elements to radiate in the longitudinal direction simultaneously. Also, all MIMO elements' ground planes are connected to get shared one common ground plane for all antennas of the MIMO system using copper-clad tape as shown in the fabricated prototype in Fig. 7. K connector, which supports the operation up to 40 GHz, is used in the MIMO system to facilitate the combining of the four elements structure.

Different parameters are used to evaluate MIMO system performance. Envelope correlation coefficient (ECC) and diversity gain (DG) are the most common parameters to estimate the isolation between the MIMO array elements. ECC measures the separation of the radiation patterns of the antenna array elements of MIMO systems. ECC is estimated employing uniform wave using field-based method depending on antennas radiation characteristics, which provides the most accurate results, as displayed by (1) [26]. Where **F** is the radiated field vector of the "mth" and "nth" antenna array element. "m" and "n" represent the port numbers. While DG defines the independence of the elements for the MIMO system and can be calculated from (2). For totally uncorrelated antenna elements, which means they have a zero value of ECC, the ideal diversity gain is 10dB.

$$ECC = \frac{\left| \iint \left[\boldsymbol{F}_m(\theta,\phi) \cdot \boldsymbol{F}_n(\theta,\phi) \right] d\Omega \right|^2}{\iint \left| \boldsymbol{F}_m(\theta,\phi) \right|^2 d\Omega \cdot \iint \left| \boldsymbol{F}_n(\theta,\phi) \right|^2 d\Omega} \quad (1)$$

$$DG = 10\sqrt{1 - |ECC|^2} \quad (2)$$

V. RESULTS OF MIMO SYSTEM

The mutual coupling between planar four-element MIMO array for the proposed antenna is calculated, as demonstrated in Fig. 8. The planar MIMO array gives lower isolation at the two operating bands, with −23 and −22 dB at 24.5 and 28.5 GHz, respectively. To verify the effectiveness of using the cross-shaped structure to increase the isolation between MIMO array elements, the S-parameters of the cross-shaped structure are calculated, as illustrated in Fig. 9. Due to the symmetry of the cross-shaped MIMO system, we measured only the S11 for one port (Port 1), and the power is sent from port 1, while the mutual coupling is measured at the other three ports (Port 2, Port 3, and Port 4). The minimum measured values of the isolation are −35, −33 dB at the lower and higher frequency bands, respectively. The measured isolation values reach up to in average −50 dB at the two resonant frequencies. Thus, the cross-shaped structure provides about an 11 dB improvement in isolation between the MIMO array elements. This enhancement can also be achieved by a planar MIMO structure, but it requires a high isolation distance between antennas, which can reach up to 60 mm. The reflection coefficient results of the cross-shaped MIMO are also shown in Fig. 9(a); the proposed MIMO system shows good matching results at the two bands.

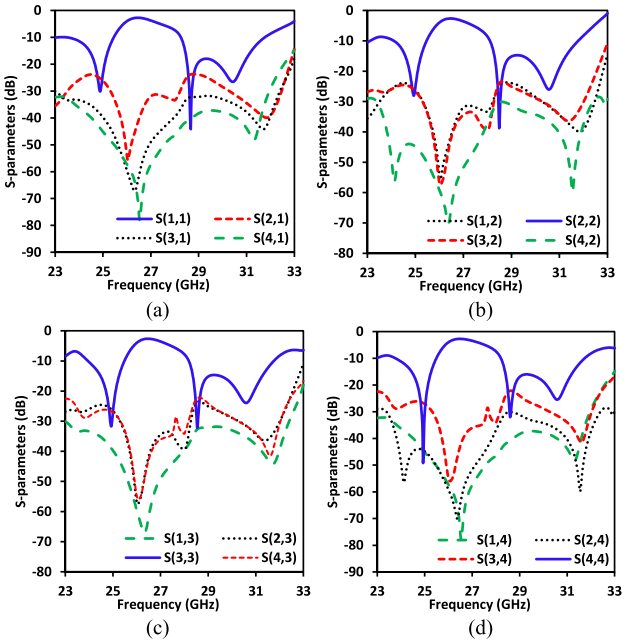

FIGURE 8. Simulated S-parameters of the planar MOMO system (a) port 1 excitation, (b) port 2 excitation, (c) port 3 excitation, and (d) port 4 excitation.

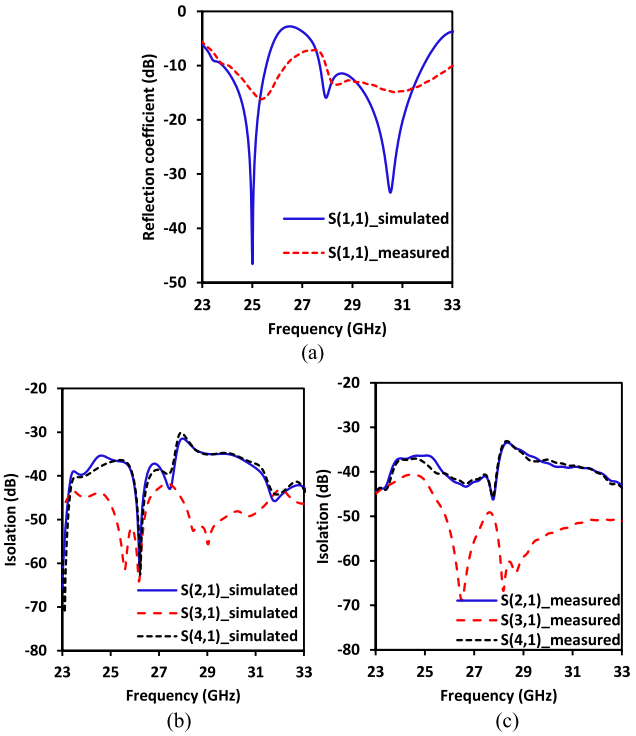

FIGURE 9. Measured and simulated results of the reflection coefficients as well as isolations of the proposed cross-shaped MIMO system (a) reflection coefficient, (b) simulated results of the isolation, and (c) measured results of the isolation.

2D and 3D normalized radiation patterns of the cross-shaped MIMO array at the two operating frequencies are displayed in Figs. 10 and 11. The array gain and radiation

TABLE 1. Comparison of the proposed mimo system with recently published mimo systems.

Ref.	Antenna type	No. of ports	Frequency (GHz)	Antenna gain	Radiation efficiency (%)	Minimal isolation (dB)
[16]	Metasurface-based antenna	2	2.43, 3.46, and 5.52	5.49, 4.57, and 0.8	32.2, 51, and 68.9	17, 18, and 32
[17]	Split-ring resonator	2	3.54, and 6.33	3.25, and 3.4	75.1, and 74.2	15
[18]	Monopole radiators with metasurface reflector	2	2.6	7.02	82.3	14.5
[27]	DRA	2	29.5-31	7	-	30
[28]	DRA	4	5.15-5.35	4.9, and 7.2	89, and 81	22
[29]	Protrudent-shaped	2	2.87 -17	<6	-	21
[19]	Loop	10	3.5	4.2- 5.9	>65	10
This work	Split ring resonators	4	24.5 and 28.5	7.9, and 7.5	92, and 95	35, and 33

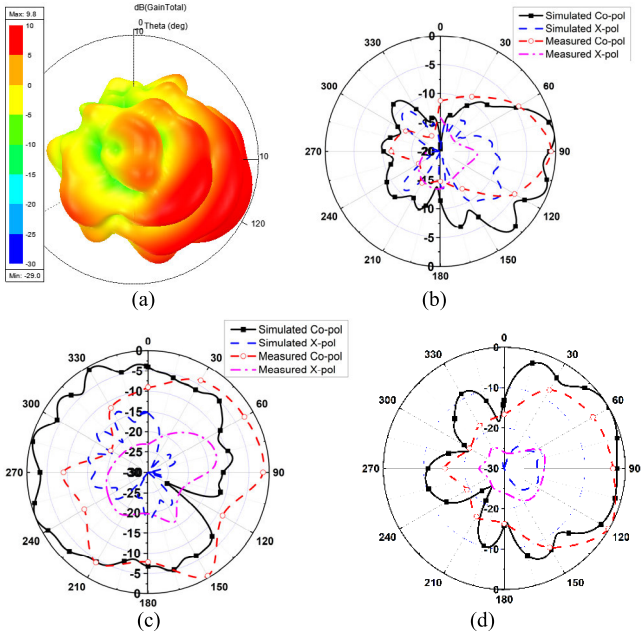

FIGURE 10. 3D and normalized 2D polar plots of the radiation patterns for MIMO system at f_1 (a) 3D radiation pattern (b) 2D at $\theta = 90°$, (c) 2D at $\phi = 0°$, (d) 2D at $\phi = 90°$.

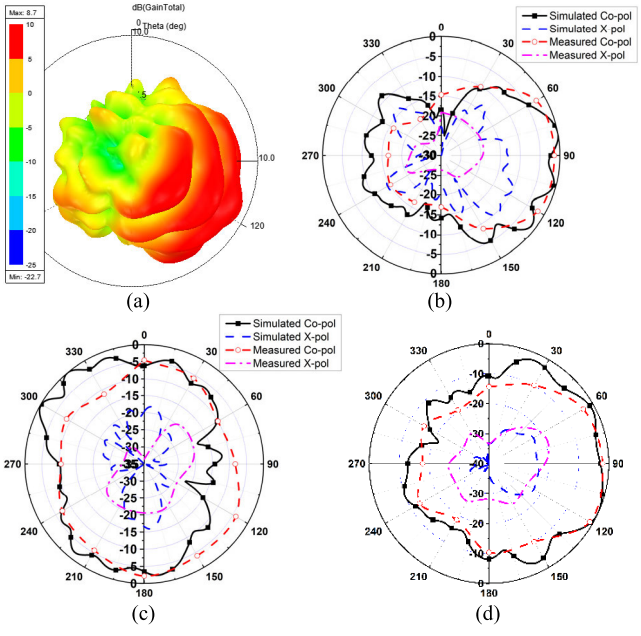

FIGURE 11. 3D and normalized 2D polar plots of the radiation patterns for MIMO system at f2 (a) 3D radiation pattern (b) 2D at $\theta = 90°$, (c) 2D at $\phi = 0°$, (d) 2D at $\phi = 90°$.

efficiency at 24.5 GHz are 9.8dB and 93%, respectively. While at 28.5 GHz, they are 8.7dB and 95%, respectively. ECC and diversity gain are calculated for two antennas with the same polarization (Antenna 1 and Antenna 3) as well as for two antennas with orthogonal polarization (Antenna 1 and Antenna 2). Fig. 12 illustrates the measured and simulated results of the array gain and the radiation efficiency versus the operating frequencies. The array gives measured gains and radiation efficiencies of 9.7 dB, 8.59 dB and 92.3%, 94% at the two radiating frequencies, respectively. Fig. 13 shows ECC and DG performance. ECC values are less than 0.0001 over the two operating bands of the proposed cross-shaped MIMO antenna, which is much lower than the accepted value of 0.5. The DG is approximately 10 over

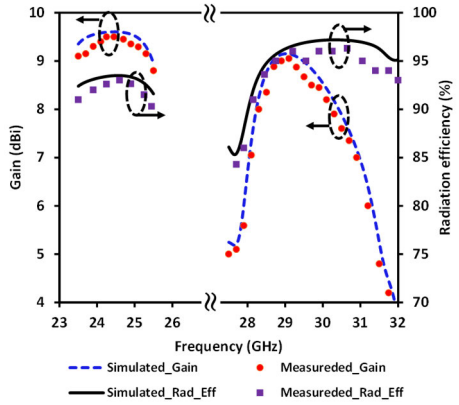

FIGURE 12. Measured and simulated outcomes of the MIMO system's gain and radiation efficiency as a function of the frequency.

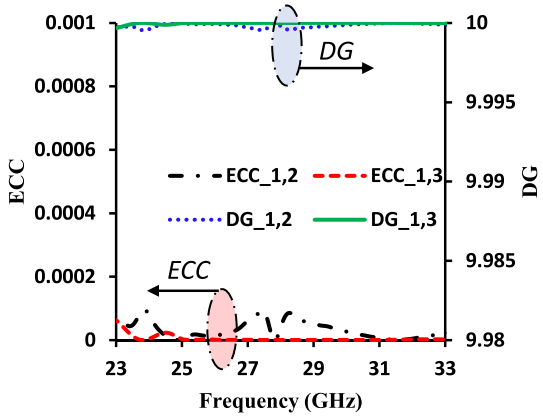

FIGURE 13. Envelope correlation coefficient in addition to diversity gain results for the proposed cross-shaped MIMO system.

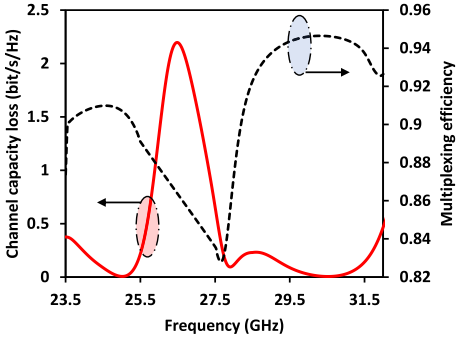

FIGURE 14. Chanel capacity loss and multiplexing efficiency of the proposed MIMO system versus the operating frequency.

the two operating bands. Furthermore, the presence of a correlation factor in MIMO antennas leads to an increase in channel capacity loss (CCL) and a decrease in multiplexing efficiency. To ensure that CCL and multiplexing efficiency remain within permissible values, they are estimated using ANSYS HFSS, as shown in Fig 14. A comparison with the state-of-the-art MIMO systems is summarized in Table 1. The proposed cross-shaped MIMO system has high isolation. Furthermore, it has high gain and radiation efficiency at both frequency bands.

VI. CONCLUSION

A cross-shaped MIMO system was proposed for millimeter-wave 5G applications, which uses a dual-band antenna with a split ring resonator as a single element. This antenna provides end-fire radiation characteristics that are compatible with the MIMO system configuration. The MIMO system operates at 24.5 and 28.5 GHz bands, with an average gain of 9dB and a radiation efficiency reaches 95%. The MIMO performance was studied, revealing a very low envelope correlation of less than 10^{-4} and diversity gain around 10 dB over the two operating bands. Therefore, a high-isolation dual-band cross-shaped MIMO array is proposed for mm-wave 5G applications. The proposed design can be used with various devices operating at the 24 GHz and 28 GHz bands, including handheld devices that require higher data rates, where spatial multiplexing can improve the signal quality of these devices.

REFERENCES

[1] Y. Q. Hei, J. G. He, and W. T. Li, "Wideband decoupled 8-element MIMO antenna for 5G mobile terminal applications," *IEEE Antennas Wireless Propag. Lett.*, vol. 20, no. 8, pp. 1448–1452, Aug. 2021.

[2] S. S. Jehangir and M. S. Sharawi, "A compact single-layer four-port orthogonally polarized Yagi-like MIMO antenna system," *IEEE Trans. Antennas Propag.*, vol. 68, no. 8, pp. 6372–6377, Aug. 2020.

[3] J. Dong, S. Wang, and J. Mo, "Design of a twelve-port MIMO antenna system for multi-mode 4G/5G smartphone applications based on characteristic mode analysis," *IEEE Access*, vol. 8, pp. 90751–90759, 2020.

[4] M. Aboualalaa, I. Mansour, H. Elsadek, A. B. Abdel-Rahman, A. Allam, M. Abo-Zahhad, K. Yoshitomi, and R. K. Pokharel, "Independent matching dual-band compact quarter-wave half-slot antenna for millimeter-wave applications," *IEEE Access*, vol. 7, pp. 130782–130790, 2019.

[5] A. B. Abdel-Rahman and M. Aboualalaa, "Improving isolation between antenna array elements using lossy microstrip resonators," in *Proc. 13th Eur. Conf. Antennas Propag. (EuCAP)*, Mar. 2019, pp. 1–4.

[6] S. Chen, L. Chou, Chung-I. G. Hsu, and S. Li, "Compact sub-6-GHz four-element MIMO slot antenna system for 5G tablet devices," *IEEE Access*, vol. 8, pp. 154652–154662, 2020.

[7] F. Liu, J. Guo, L. Zhao, G. Huang, Y. Li, and Y. Yin, "Dual-band metasurface-based decoupling method for two closely packed dual-band antennas," *IEEE Trans. Antennas Propag.*, vol. 68, no. 1, pp. 552–557, Jan. 2020.

[8] L. Sun, Y. Li, Z. Zhang, and H. Wang, "Self-decoupled MIMO antenna pair with shared radiator for 5G smartphones," *IEEE Trans. Antennas Propag.*, vol. 68, no. 5, pp. 3423–3432, May 2020.

[9] M. Sharma, R. Kumar, P. Kaur, V. Dhasarathan, and T. K. Nguyen, "Design and analysis of on-demand reconfigurable WiMAX/WLAN high isolation 2×2 MIMO antenna oriented adjacent/orthogonally for imaging applications in UWB-X band," *Int. J. RF Microw. Comput.-Aided Eng.*, vol. 32, no. 1, Jan. 2022, Art. no. e22928.

[10] W. Hu, L. Qian, S. Gao, L. Wen, Q. Luo, H. Xu, X. Liu, Y. Liu, and W. Wang, "Dual-band eight-element MIMO array using multi-slot decoupling technique for 5G terminals," *IEEE Access*, vol. 7, pp. 153910–153920, 2019.

[11] L. Chang, Y. Yu, K. Wei, and H. Wang, "Polarization-orthogonal co-frequency dual antenna pair suitable for 5G MIMO smartphone with metallic bezels," *IEEE Trans. Antennas Propag.*, vol. 67, no. 8, pp. 5212–5220, Aug. 2019.

[12] M. Li, Y. Ban, Z. Xu, G. Wu, C. Sim, K. Kang, and Z. Yu, "Eight-port orthogonally dual-polarized antenna array for 5G smartphone applications," *IEEE Trans. Antennas Propag.*, vol. 64, no. 9, pp. 3820–3830, Sep. 2016.

[13] N. O. Parchin, Y. I. A. Al-Yasir, A. H. Ali, I. Elfergani, J. M. Noras, J. Rodriguez, and R. A. Abd-Alhameed, "Eight-element dual-polarized MIMO slot antenna system for 5G smartphone applications," *IEEE Access*, vol. 7, pp. 15612–15622, 2019.
[14] Z. Ren, A. Zhao, and S. Wu, "MIMO antenna with compact decoupled antenna pairs for 5G mobile terminals," *IEEE Antennas Wireless Propag. Lett.*, vol. 18, no. 7, pp. 1367–1371, Jul. 2019.
[15] K.-L. Wong, M.-F. Jian, C.-J. Chen, and J.-Z. Chen, "Two-port same-polarized patch antenna based on two out-of-phase TM_{10} modes for access-point MIMO antenna application," *IEEE Antennas Wireless Propag. Lett.*, vol. 20, no. 4, pp. 572–576, Apr. 2021.
[16] M. Ameen, O. Ahmad, and R. K. Chaudhary, "Bandwidth and gain enhancement of triple-band MIMO antenna incorporating metasurface-based reflector for WLAN/WiMAX applications," *IET Microw., Antennas Propag.*, vol. 14, no. 13, pp. 1493–1503, Oct. 2020.
[17] M. Ameen, O. Ahmad, and R. K. Chaudhary, "Single split-ring resonator loaded self-decoupled dual-polarized MIMO antenna for mid-band 5G and C-band applications," *AEU - Int. J. Electron. Commun.*, vol. 124, Sep. 2020, Art. no. 153336.
[18] M. Ameen, O. Ahmad, and R. K. Chaudhary, "Wideband circularly-polarised high-gain diversity antenna loaded with metasurface reflector for small satellite applications," *Electron. Lett.*, vol. 55, no. 15, pp. 829–831, Jul. 2019.
[19] I. R. R. Barani, K.-L. Wong, Y.-X. Zhang, and W.-Y. Li, "Low-profile wideband conjoined open-slot antennas fed by grounded coplanar waveguides for 4 × 4 5 g MIMO operation," *IEEE Trans. Antennas Propag.*, vol. 68, no. 4, pp. 2646–2657, Apr. 2020.
[20] P. K. Patra and M. K. Das, "Modified ground with 50 ω step fed WLAN notch 2 × 2 MIMO UWB antenna," *Int. J. RF Microw. Comput.-Aided Eng.*, vol. 30, no. 3, pp. 1–14, Mar. 2020.
[21] H. Piao, Y. Jin, Y. Xu, and L. Qu, "MIMO ground-radiation antennas using a novel closed-decoupling-loop for 5G applications," *IEEE Access*, vol. 8, pp. 142714–142724, 2020.
[22] S. S. Alja'afreh, B. Altarawneh, M. H. Alshamaileh, E. R. Almajali, R. Hussain, M. S. Sharawi, L. Xing, and Q. Xu, "Ten antenna array using a small footprint capacitive-coupled-shorted loop antenna for 3.5 GHz 5G smartphone applications," *IEEE Access*, vol. 9, pp. 33796–33810, 2021.
[23] Z. Xu and C. Deng, "High-isolated MIMO antenna design based on pattern diversity for 5G mobile terminals," *IEEE Antennas Wireless Propag. Lett.*, vol. 19, no. 3, pp. 467–471, Mar. 2020.
[24] S. P. Biswal and S. Das, "A compact printed ultra-wideband multiple-input multiple-output prototype with band-notch ability for WiMAX, LTE-band43, and WLAN systems," *Int. J. RF Microw. Comput. Eng.*, vol. 29, no. 6, pp. 1–11, 2019.
[25] Z. Du, X. Zhang, P. Qin, Y. Pu, and X. Xi, "Intercoupling suppression of very closely spaced MIMO antenna based on current cancellation method," *IEEE Access*, early access, Nov. 24, 2022, doi: 10.1109/ACCESS.2022.3224461.
[26] S. Blanch, J. Romeu, and I. Corbella, "Exact representation of antenna system diversity performance from input parameter description," *Electron. Lett.*, vol. 39, no. 9, pp. 705–707, May 2003.
[27] M. S. Sharawi, S. K. Podilchak, M. T. Hussain, and Y. M. M. Antar, "Dielectric resonator based MIMO antenna system enabling millimetre-wave mobile devices," *IET Microw., Antennas Propag.*, vol. 11, no. 2, pp. 287–293, Jan. 2017.
[28] G. Das, N. K. Sahu, A. Sharma, R. K. Gangwar, and M. S. Sharawi, "FSS-based spatially decoupled back-to-back four-port MIMO DRA with multidirectional pattern diversity," *IEEE Antennas Wireless Propag. Lett.*, vol. 18, no. 8, pp. 1552–1556, Aug. 2019.
[29] A. K. Gautam, A. Saini, N. Agrawal, and N. Z. Rizvi, "Design of a compact protrudent-shaped ultra-wideband multiple-input-multiple-output/diversity antenna with band-rejection capability," *Int. J. RF Microw. Comput.-Aided Eng.*, vol. 29, no. 9, pp. 1–11, Sep. 2019.

MOHAMED ABOUALALAA (Member, IEEE) received the M.S. degree in electronics and communications engineering from Cairo University, Egypt, in 2014, and the Ph.D. degree in electronics and communications engineering from the Egypt–Japan University of Science and Technology (E-JUST), Alexandria, Egypt, in 2018. From 2010 to 2013, he was a Research Assistant with the Microstrip Circuits Department, Electronics Research Institute, Cairo, Egypt, where he was an Assistant Researcher, from 2014 to 2015. He was a Special Research Student with Kyushu University, Japan, from 2017 to 2018, where he was a Postdoctoral Research Fellow with the Egypt–Japan Education Partnership (EJEP) Program, from 2019 to 2020. He is currently an Assistant Professor with the Electronics Research Institute. His research interests include microwave planar antennas, reconfigurable antennas, energy harvesting, and wireless power transfer. He is a member of the editorial board of the *Journal of Electrical and Electronic Engineering*.

ISLAM MANSOUR received the B.Sc. degree in electrical and electronic engineering from Benha University, Cairo, Egypt, in 2010, the M.Sc. degree in electrical and electronic engineering from Ain Shams University, Cairo, in 2015, and the Ph.D. degree in electrical and electronic engineering from the Egypt–Japan University of Science and Technology (EJUST), Egypt, in 2019. She was the Ph.D. student of channel with the Faculty of Information Science and Electrical Engineering, Kyushu University, Fukuoka, Japan, from 2017 to 2018. She is currently an Assistant Professor with the Electrical Department, Faculty of Engineering Shoubra, Benha University, Egypt. She is involved in millimeter-wave frequency generation circuit design and its applications.